ARTICLE

Stabilisation of $[WF_5]^+$ and WF_5 by Pyridine: Facile Access to $[WF_5(NC_5H_5)_3]^+$ and $WF_5(NC_5H_5)_2$

Douglas Turnbull[a], Paul Hazendonk[a], Stacey D. Wetmore[a], Michael Gerken*[a]

Abstract: The enhanced reactivity of $[WF_5]^+$ over WF_6 has been exploited to access a neutral derivative of elusive WF_5. The reaction of $WF_6(NC_5H_5)_2$ with $[(CH_3)_3Si(NC_5H_5)][O_3SCF_3]$ in CH_2Cl_2 results in quantitative formation of trigonal-dodecahedral $[WF_5(NC_5H_5)_3]^+$, which has been characterised as its $[O_3SCF_3]^-$ salt by Raman spectroscopy in the solid state and variable-temperature NMR spectroscopy in solution. The salt is susceptible to slow decomposition in solution at ambient temperature via dissociation of a pyridyl ligand, and the resultant $[WF_5(NC_5H_5)_2]^+$ is reduced to $WF_5(NC_5H_5)_2$ in the presence of excess C_5H_5N, as determined by ^{19}F NMR spectroscopy. Pentagonal-bipyramidal $WF_5(NC_5H_5)_2$ was isolated and characterised by X-ray crystallography and Raman spectroscopy in the solid state, representing the first unambiguously characterised WF_5 adduct, as well as the first heptacoordinate adduct of a transition-metal pentafluoride. Density-functional-theory (DFT-B3LYP) methods have been used to investigate the reduction of $[WF_5(NC_5H_5)_2]^+$ to $WF_5(NC_5H_5)_2$, supporting a two-electron reduction of W^{VI} to W^{IV} via nucleophilic attack and deprotonation of a pyridyl ligand in the presence of free C_5H_5N, followed by comproportionation to W^V.

1 Introduction

The transition-metal hexafluorides are regarded for their capabilities as powerful oxidising and fluorinating agents. Platinum hexafluoride, one of the strongest oxidising agents known, is famously capable of spontaneously oxidising O_2 to $[O_2]^+$[1] and Xe to $[XeF]^+$.[2,3] Its reactions with the F^- donors NOF and NO_2F resulted in spontaneous generation of F_2,[4,5] and a computational study of $[PtF_7]^-$ suggests instability towards decomposition to $[PtF_6]^-$ and F^-.[6]

In some cases, however, such as the reaction of C_6F_6 with OsF_6,[7] or of Xe with IrF_6,[8] even these strong oxidising agents are insufficient to react with certain substrates. Under such circumstances, addition of SbF_5 to the reaction mixture has been observed to enhance the electron affinity (EA) of the metal centre. This has allowed for the synthesis of $[C_6F_6][Os_2F_{11}]$[7] and the low-temperature preparation of $[XeF][IrSbF_{11}]$.[8] Similarly, reaction of the actinide congener UF_6 with SbF_5 in $C_2F_4Cl_2$ resulted in an unexpected oxidation of the (typically inert) solvent to yield $UF_5{\cdot}2SbF_5$.[9]

It could be envisioned that SbF_5, a strong F^- acceptor, elicits F^- donation from MF_6 to form a reactive intermediate with $[MF_5]^+$ character. Fluorine-19 and Raman spectroscopic studies of UF_6 in SbF_5 vaguely suggested withdrawal of electron density from the U^{VI} centre, though no discrete ionic species could be identified.[9] Indeed, these M–F···Sb interactions seem to be tenuous, considering that WF_6 was employed as an inert solvent for reactions of SbF_5 with BiF_5.[10,11] No discrete $[MF_5]^+$ cation, or derivative thereof, had been reported until the recent syntheses of $[WF_5(2,2'\text{-bipy})][Sb_2F_{11}]$ and $[WF_5(1,10\text{-phen})][Sb_nF_{5n+1}]$ (n = 1, 2) via reactions of $WF_6(L)$ (L = 2,2′-bipy, 1,10-phen) with $SbF_5(OSO)$ in SO_2.[12] These salts were found to be thermally stable and their crystal structures revealed "monocapped-4:3" coordination spheres about the W^{VI} centres upon consideration of the weak cation-anion contacts.

These donor-stabilised $[WF_5]^+$ complexes are predicted to behave as significantly stronger oxidising agents than WF_6.[12] Their reduction could serve as an alternative synthetic route to thermally unstable WF_5, the cumbersome preparations of which involve reduction of WF_6 with W wires at 500–700 °C in a cold (–50 to –60 °C) quartz vessel[13,14] or F^- abstraction from $[WF_6]^-$ in HF/SbF_5, followed by sublimation at 0°C.[15] Alternatively, neutral derivatives thereof could be prepared, as hitherto none have been characterised definitively. Herein, we demonstrate that F^- abstraction from WF_6 in the presence of C_5H_5N can be achieved under relatively mild conditions using $(CH_3)_3SiO_3SCF_3$, and that decomposition of the resultant $[WF_5(NC_5H_5)_3]^+$ cation in C_5H_5N results in controlled reduction to $WF_5(NC_5H_5)_2$.

2 Results and Discussion

2.1 Syntheses and Physical Properties of $[WF_5(NC_5H_5)_3][O_3SCF_3]$ and $WF_5(NC_5H_5)_2$

The reaction of $WF_6(NC_5H_5)_2$ with one molar equivalent of $[(CH_3)_3Si(NC_5H_5)][O_3SCF_3]$ in CH_2Cl_2 at –60 °C resulted in F^- abstraction, quantitatively yielding $[WF_5(NC_5H_5)_3]^+$ (Eq. 1). The $[WF_5(NC_5H_5)_3][O_3SCF_3]$ salt was isolated as a colourless solid upon removal of the volatile materials under dynamic vacuum. It is highly soluble in SO_2ClF, SO_2 and CH_2Cl_2, though the solutions turn brown over several hours at ambient temperature due to decomposition, and it is insoluble in $CFCl_3$.

$$WF_6(NC_5H_5)_2 + [(CH_3)_3Si(NC_5H_5)]^+ \rightarrow [WF_5(NC_5H_5)_3]^+ + (CH_3)_3SiF \quad (1)$$

Attempts to prepare $[WF_5(NC_5H_5)_2][O_3SCF_3]$ via reaction of $WF_6(NC_5H_5)$ and $[(CH_3)_3Si(NC_5H_5)][O_3SCF_3]$, or $[WF_5(NC_5H_5)_2][Sb_2F_{11}]$ via reaction of $WF_6(NC_5H_5)_2$ with

[a] D. Turnbull, Prof. Dr. P. Hazendonk, Prof. Dr. S. D. Wetmore, Prof. Dr. M. Gerken
Canadian Centre for Research in Advanced Fluorine Technologies and Department of Chemistry and Biochemistry
University of Lethbridge
4401 University Drive
Lethbridge, AB
T1K 3M4
(Canada)
E-mail: michael.gerken@uleth.ca

Supporting information for this article is given via a link at the end of the document.

$SbF_5(OSO)$ in SO_2 did not yield a sole, identifiable product. Monitoring the attempted preparation of $[WF_5(NC_5H_5)_2][Sb_2F_{11}]$ by ^{19}F NMR spectroscopy revealed the instability of the heptacoordinate cation (*vide infra*).

The attempted preparation of $[WF_5(NC_5H_5)_3][O_3SCF_3]$ in excess C_5H_5N resulted in the formation of a pale yellow solution, which over time darkened to red-brown. After 16–24 h at ambient temperature, red-orange crystals settled from what had become an intractable oil. These crystals were isolated after washing with CH_2Cl_2 and found to consist of $WF_5(NC_5H_5)_2$ by X-ray crystallography, though their Raman spectrum revealed significant contamination by $WF_6(NC_5H_5)_2$. This impurity could be minimised by employing a slight excess of $(CH_3)_3SiO_3SCF_3$ (1.1 equiv.), agitating the mixture after 16–24 h at ambient temperature, allowing to settle for an additional 24 h, and subsequently washing with CH_2Cl_2. Under these conditions, $WF_5(NC_5H_5)_2$ could be obtained in *ca.* 60% yield. If 1.5 molar equivalents of $(CH_3)_3SiO_3SCF_3$ were employed, the yield was drastically reduced (< 20%). The $WF_5(NC_5H_5)_2$ adduct was found to be slightly soluble in CH_2Cl_2, C_5H_5N and CH_3CN.

Both $[WF_5(NC_5H_5)_3][O_3SCF_3]$ and $WF_5(NC_5H_5)_2$ are thermally stable in the solid state under an atmosphere of dry N_2. This is especially noteworthy for $WF_5(NC_5H_5)_2$, as it contrasts with the proclivity of WF_5 to disproportionate at ambient or slightly elevated temperatures.[13,14] They are, however, hydrolytically sensitive. In the latter case, exposure to air, H_2O, or aqueous NaOH results in blue/violet discolouration due to the formation of mixed-oxidation-state tungsten oxides.[16]

2.2 Molecular Structures

The $WF_5(NC_5H_5)_2$ adduct was found to crystallise from the mother liquor during preparation and could also be recrystallised from hot CH_3CN, allowing for determination of its structure via X-ray crystallography at –161 °C. Crystallographic data collection and refinement parameters are given in Table S1. While attempts to grow crystals of $[WF_5(NC_5H_5)_3][O_3SCF_3]$ were unsuccessful, the geometry of the cation was determined unambiguously by variable-temperature ^{19}F NMR spectroscopy (*vide infra*). In addition, gas-phase structures were optimised for $WF_5(NC_5H_5)_2$ and $[WF_5(NC_5H_5)_n]^+$ (n = 2, 3) at the B3LYP/aVTZ level of theory. Selected experimental and calculated metric parameters are listed in Figures 1 and 2 as well as Tables S2 and S3.

2.2.1 $WF_5(NC_5H_5)_2$

The $WF_5(NC_5H_5)_2$ adduct crystallises in the monoclinic space group $C2/c$ (a = 8.1621(4) Å, b = 11.1419(5) Å, c = 13.6465(7) Å, β = 107.055(6)°, Z = 4, R_1 = 0.0099, wR_2 = 0.0234), adopting a pentagonal-bipyramidal geometry with crystallographically imposed C_2 symmetry, in which the nitrogen atoms occupy non-adjacent, equatorial positions (Figure 1). The pentagonal plane is nearly ideal, with only small displacements from the least-squares plane (< 0.08 Å), an ideal sum of internal angles (exptl. 360.3°, calcd. 360.4°), and no displacement of the tungsten centre from the plane. A similar coordination geometry has been observed for the adducts of WOF_4[17,18] and $W(NC_6F_5)F_4$[18] with two molar equivalents of C_5H_5N. Adducts of WOF_4 with chelating diphosphines are also pentagonal-bipyramidal; however, the donor atoms occupy adjacent sites in the pentagonal plane.[19] The $WXF_4(NC_5H_5)_2$ (X = O, F) adducts are isomorphic, but can be distinguished by their unit-cell parameters ($WOF_4(NC_5H_5)_2$: a = 8.2014(5) Å, b = 11.1972(5) Å, c = 13.5387(9) Å, β = 107.256(7)°) and disorder between the axial W=O and W–F bonds in $WOF_4(NC_5H_5)_2$ resulting in an averaged bond length (1.834(2) Å).[18] To our knowledge, only one other heptacoordinate fluoridotungsten(V) complex is known, i.e., $K_2[WF_7]$, in which the anion is found to adopt an edge-disordered, monocapped-trigonal-prismatic geometry.[20]

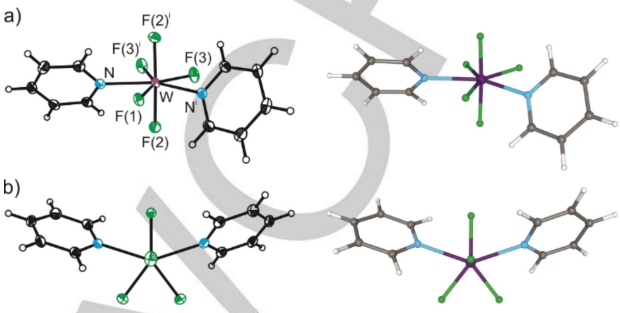

Figure 1. Thermal ellipsoid plots (50% probability level, left) and optimised gas-phase structures (B3LYP/aVTZ, right) of a) side-on and b) top-down views of $WF_5(NC_5H_5)_2$. Selected experimental [calculated] bond lengths (Å) and angles (°): W–F(1) 1.8936(14) [1.904], W–F(2) 1.9088(12) [1.920], W–F(3) 1.9191(11) [1.902], W–N 2.2206(15) [2.294], F(1)–W–F(2) 87.49(3) [85.9], F(1)–W–F(3) 143.14(3) [142.1], F(1)–W–N 72.14(4) [71.3], F(2)–W–F(2)^i 174.98(7) [171.9], F(3)–W–F(3)^i 73.72(7) [75.8], N–W–N^i 144.27(7) [142.5]. Symmetry transformation: i = 1 – x, y, ½ – z.

Comparison of $WF_5(NC_5H_5)_2$ and $[WF_7]^{2-}$ reveal insignificant differences between their W–F bond lengths (1.8936(14)–1.9191(11) and 1.882(16)–1.95(7) Å)[20], respectively), though large errors in the latter prevent more precise analysis. In addition, the W–F bonds are typically elongated relative to those of comparable heptacoordinate W^{VI} complexes such as $WF_6(NC_5H_5)$ and its derivatives (1.803(8)–1.880(6) Å)[21,22] as well as $[WF_5(L)]^+$ (L = 2,2′-bipy, 1,10-phen; 1.8377(19)–1.861(3) Å).[12] In contrast, the W–N bonds (2.2206(15) Å) in $WF_5(NC_5H_5)_2$ are insignificantly different from, or even slightly shorter than, those of the aforementioned W^{VI} complexes (2.214(3)–2.294(9) Å).

In comparison to the most closely related neutral W^V adduct, *trans*-$WF_4\{N(CH_2CF_3)_2\}\{P(C_6H_5)_3\}$, the W–F bonds in $WF_5(NC_5H_5)_2$ (1.8936(14)–1.9191(11) Å) are, on average, elongated in relation to those of the bent WF_2 moiety (1.845(3)–1.859(3) Å), but differ insignificantly from those of its linear WF_2 moiety (1.884(3)–1.912(3) Å).[23] The W^V–Pn (Pn = N, P) normalised contacts[24] in $WF_5(NC_5H_5)_2$ (0.624) and *trans*-$WF_4\{N(CH_2CF_3)_2\}\{P(C_6H_5)_3\}$ (0.682) suggest stronger W–Pn bonds in the former, a trend which was also observed between WF_6 adducts with N- and P-donor ligands.[22]

The optimised gas-phase geometry of $WF_5(NC_5H_5)_2$ agrees excellently with the geometry observed in the crystal structure (Figure 1), in which the largest discrepancy is a minor overestimation of the W–N bond length (2.2206(15) vs. 2.294 Å). Whereas the longest W–F bonds in the crystal structure are W–F(3)/F(3)^i, these are the shortest W–F bonds in the optimised geometry.

The $WF_5(NC_5H_5)_2$ adduct represents the first heptacoordinate adduct of a transition-metal pentafluoride; NMR spectroscopic[25,26] and crystallographic[27] studies of $MF_5 \cdot 2C_5H_5N$ (M = Nb, Ta) revealed that MF_5 undergo quantitative ligand-induced autoionisation to the ionic coordination isomers, $[MF_4(NC_5H_5)_4][MF_6]$, upon reaction with C_5H_5N. Furthermore, the

observation of ionic species upon reactions of MF_5 with excess monodentate donor ligand, or stoichiometric amounts of bidentate ligand, is ubiquitous.[28,29] Uranium pentafluoride, however, forms a monocapped-trigonal-prismatic adduct with 2,2′-bipy;[30] $UF_5 \cdot 2HCN$ instead manifests as a one-dimensional coordination polymer with trigonal-dodecahedral U^V centres.[31]

2.2.2 $[WF_5(NC_5H_5)_n]^+$ (n = 2, 3)

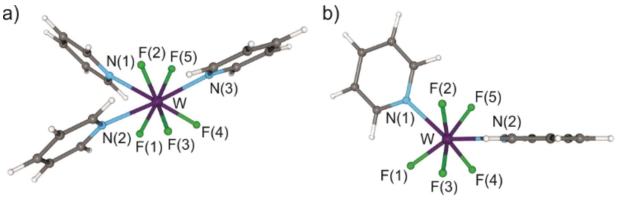

Figure 2. Optimised gas-phase structures (B3LYP/aVTZ) of a) $[WF_5(NC_5H_5)_3]^+$ and b) $[WF_5(NC_5H_5)_2]^+$. Selected bond lengths (Å) for $[WF_5(NC_5H_5)_3]^+$: W–F(1) 1.867, W–F(2) 1.878, W–F(3) 1.863, W–F(4) 1.864, W–F(5) 1.878, W–N(1) 2.398, W–N(2) 2.382, W–N(3) 2.356. Selected bond lengths (Å) for $[WF_5(NC_5H_5)_2]^+$: W–F(1) 1.846, W–F(2) 1.859, W–F(3) 1.848, W–F(4) 1.848, W–F(5) 1.859, W–N(1) 2.293, W–N(2) 2.276.

Optimisation of the gas-phase structures of $[WF_5(NC_5H_5)_n]^+$ (n = 2, 3) resulted in monocapped-trigonal-prismatic and trigonal-dodecahedral geometries, respectively. In $[WF_5(NC_5H_5)_3]^+$, the nitrogen atoms and one fluorido ligand occupy the "A" coordination sites of the trigonal dodecahedron and the remaining fluorido ligands correspondingly occupy the "B" (equatorial) sites (Figure 2a).[32] This was achieved even when a bicapped-trigonal-prismatic geometry derived from the crystal structure of $WF_6(NC_5H_5)_2$ was input as the starting geometry for the optimisation. The cation possesses C_1 symmetry, though the WF_5N_3 moiety approximates C_s symmetry.

In $[WF_5(NC_5H_5)_2]^+$, the geometry is monocapped-trigonal-prismatic in which the nitrogen atoms occupy the capping position and one vertex opposite the capping position, resulting in overall C_s symmetry (Figure 2b). This geometry contrasts with those of the $[WF_5(L)]^+$ (L = 2,2′-bipy, 1,10-phen) cations, in which the presence of bidentate ligands yields monocapped-octahedral or 4:3-polyhedral geometries. An attempt to optimise a pentagonal-bipyramidal (C_2-symmetric) stereoisomer based on that of $WF_5(NC_5H_5)_2$ resulted in a transition state that is 6 kJ mol^{-1} higher in energy, in which the imaginary frequency corresponds to a distortion towards the ground-state structure.

The W–F bond lengths are predicted to be significantly longer in $[WF_5(NC_5H_5)_3]^+$ (1.863–1.878 Å) than in $[WF_5(NC_5H_5)_2]^+$ (1.846–1.856 Å) and $[WF_5(L)]^+$, though not as long as in $WF_5(NC_5H_5)_2$. Similarly, the W–N bonds in $[WF_5(NC_5H_5)_3]^+$ (2.356–2.398 Å) are significantly longer than in any of the aforementioned heptacoordinate complexes, including $WF_5(NC_5H_5)_2$. These trends in W–F and W–N bond lengths are attributed primarily to significantly increased steric crowding caused by octacoordination. As expected, the W–F and W–N bond lengths are highly comparable between $[WF_5(NC_5H_5)_2]^+$ and $[WF_5(L)]^+$.

2.3 Raman Spectroscopy

The ambient-temperature Raman spectra of solid $[WF_5(NC_5H_5)_3][O_3SCF_3]$ and $WF_5(NC_5H_5)_2$ (Figure 3) were obtained and vibrational frequencies were calculated for the optimised gas-phase structures, resulting in excellent agreement between the experimental and calculated data. Experimental and calculated vibrational frequencies, with assignments, are given in Tables S4 and S5. Bands corresponding to $[O_3SCF_3]^-$ were identified by comparison to those of aqueous HO_3SCF_3.[33]

In $[WF_5(NC_5H_5)_3][O_3SCF_3]$, the $\nu_s(WF_5)$ frequency (in cm^{-1}; exptl. 667, calcd. 679) is consistent with octacoordinate W^{VI} complexes such as $WF_6(NC_5H_5)_2$ (exptl. 661,[34] calcd. 673[12]), $WF_6(L)$ (L = 2,2′-bipy, 1,10-phen; exptl. 647–665, calcd. 661–692), and $[WF_4(2,2'\text{-bipy})_2]^{2+}$ (exptl. 645, 687;[35] calcd. 650, 684[12]). Two $\nu_s(NC_5)$ modes with significant Raman activity were predicted, one corresponding to the symmetric coupling of the N(1)- and N(2)-pyridyl ligands (1036), and the other to that of the N(3)-pyridyl ligand (1038). Due to their highly similar frequencies, only one $\nu_s(NC_5)$ band was observed experimentally. The $\nu_s(NC_5)$ modes (exptl. 1022; calcd. 1036, 1038) are blue-shifted from that of free C_5H_5N (exptl. 990, calcd. 1013) to a similar extent as in $WF_6(NC_5H_5)$ (exptl. 1024,[22,34] calcd. 1041[22]) and $WF_6(NC_5H_5)_2$ (exptl. 1026,[34] calcd. 1036[12]). Three distinct W–N stretching modes, $\nu_{as}(WN_3)$ (168), $\nu_s(WN_3)$ (151), and $\nu_{as}(WN_2)$ (130) are predicted, the last of which is tentatively assigned to a band at 175 cm^{-1} (*cf.* $WF_6(NC_5H_5)$: exptl. 198, calcd. 161).[22]

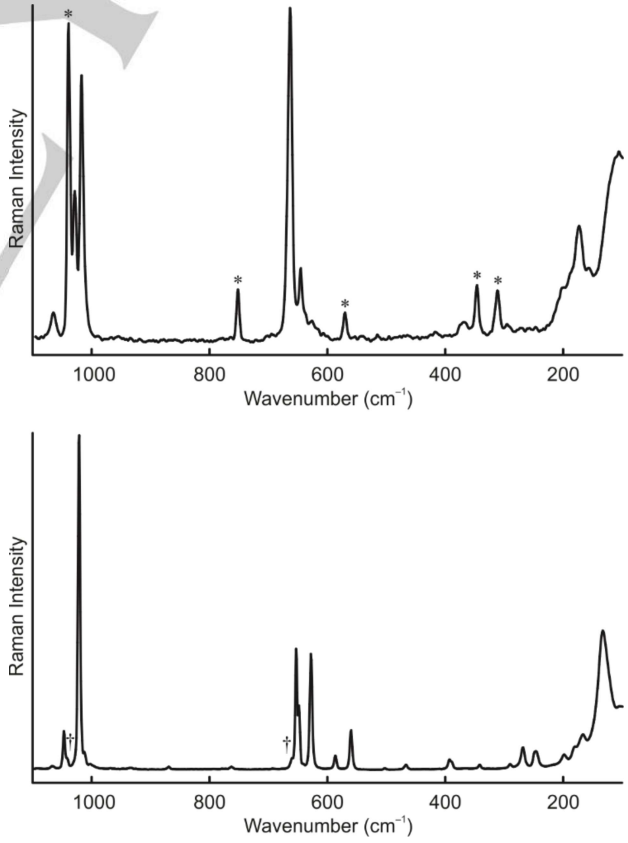

Figure 3. Raman spectra of solid $[WF_5(NC_5H_5)_3][O_3SCF_3]$ (top) and $WF_5(NC_5H_5)_2$ (bottom), recorded at ambient temperature. Asterisks (*) and daggers (†) denote $[O_3SCF_3]^-$ and $WF_6(NC_5H_5)_2$, respectively.

In $WF_5(NC_5H_5)_2$, several bands are observed between 500 and 660 cm^{-1} that are attributed to W–F stretching vibrations, which were assigned by comparison to the calculated vibrational frequencies. The $\nu_s(WF_5)$ stretch and in-plane deformations of the pyridyl ligands are coupled, resulting in two bands (exptl. 655, 630, calcd. 660, 636). The symmetric W–F_{ax} stretch, $\nu_s(WF_{2,\,ax})$, couples with stretching vibrations of the W–F_{eq} bonds, resulting in two further bands (exptl. 588, 562, calcd. 607, 555). The $\nu_s(WF_5)$ modes are similar in frequency to the $\nu_s(WF_7)$ modes of $M_2[WF_7]$[20] (M = K: 642; M = Rb: 637) but are considerably lower than the symmetric W–F stretching modes of heptacoordinate WF_6[22] or $[WF_5]^+$[12] complexes (*ca.* 700). The symmetrically (s) and antisymmetrically (as) coupled $\nu_s(NC_5)$ modes of the pyridyl ligands (exptl. 1024 (s), 1016 (as); calcd. 1040 (s), 1038 (as)) are also significantly blue-shifted. The tentatively assigned symmetric W–N stretching mode (exptl. 167, calcd. 154) is predicted to be similar to $WF_6(NC_5H_5)$.[22]

2.4 NMR Spectroscopy

2.4.1 $[WF_5(NC_5H_5)_3][O_3SCF_3]$

In CH_2Cl_2 at –100 °C, the fluorine-on-tungsten (F-on-W^{VI}) region in the ^{19}F NMR spectrum of $[WF_5(NC_5H_5)_3][O_3SCF_3]$ gives rise to an AB_2CD spin system, which was simulated and its coupling constants optimised (Table 1, Figures 4 and S5). The F_A resonance corresponds to F(1), F_B to F(3) and F(5), F_C to F(2), and F_D to F(4). Traces of $[WF_4(NC_5H_5)_4]^{2+}$ (158.63 ppm, *cf.* $[WF_4(2,2'\text{-bipy})_2]^{2+}$: 155 ppm[12,35,36]) and $WF_6(NC_5H_5)_2$[34] (122.58, 74.49 ppm) are observed at the start of the reaction, which is attributed to twofold F^- abstraction from $WF_6(NC_5H_5)_2$ causing retention of some unreacted educt (Eq. 2). The ^1H NMR spectrum reveals two distinct environments for the three pyridyl ligands (Y and Z, Figure 4). Through-space F_A–H_o(Z) (2.5 Hz) and F_C–H_o(Z) (14.0 Hz) couplings via the π systems of the Z pyridyl ligands were simulated, resulting in a heteronuclear AB_2CDX_4 spin system. The latter coupling is well resolved and gives rise to the H_o(Z) doublet of doublets (Figure 4).

Table 1. Fluorine-19 NMR Spectroscopic Data for $[WF_5(NC_5H_5)_3]^+$[a]

	$\delta(^{19}F)$ (ppm)	J (Hz)[b]		
		$^2J(F–F_B)$	$^2J(F–Fc)$	$^2J(F–F_D)$
F_A	160.70	20.9(3)	180.7(3)	53.9(4)
F_B	140.42		143.2(3)	65.4(3)
F_C	107.17			76.2(4)
F_D	105.74			

[a] Recorded in CH_2Cl_2 at –100 °C. [b] Determined via spectral simulations and optimisations using SpinWorks (version 4.2.7).[37]

$$WF_6(NC_5H_5)_2 + 2[(CH_3)_3Si(NC_5H_5)]^+ \rightarrow [WF_4(NC_5H_5)_4]^{2+} + 2(CH_3)_3SiF \quad (2)$$

Upon warming to –60 °C, coupling information within the F_B, F_C, and F_D resonances is lost and F_A collapses into a pseudo-quintet. Between –40 and –20 °C, the F_B, F_C, F_D resonances coalesce into a broad singlet (F_X) and F_A collapses to a binomial quintet with an averaged $^2J(F_A–F_X)$ (71.1 Hz), representing a pseudo-AX_4 spin system. At 20 °C, all coupling information in the F_A resonance is lost, though the F_A and F_X environments remain distinct. The coalescence event is accompanied by ^{19}F decoupling in the ^1H NMR spectrum at –60 °C such that through-space coupling is no longer observed.

At or above 0 °C, decomposition of $[WF_5(NC_5H_5)_3]^+$ is indicated by formation of a broad resonance at 155 ppm in the ^{19}F NMR spectrum along with increasing amounts of $[WF_4(NC_5H_5)_4]^{2+}$. The broad resonance is tentatively attributed to $[WF_5(NC_5H_5)_2]^+$ that undergoes rapid exchange with $[WF_5(NC_5H_5)_3]^+$ and $WF_6(NC_5H_5)_2$, and interacts with $[O_3SCF_3]^-$. Intermolecular exchange occurs to such an extent that $WF_6(NC_5H_5)_2$ is no longer observed. This explains its difference in chemical shift from the related $[WF_5(L)]^+$ cations, which are stabilised by the more weakly coordinating $[Sb_nF_{5n+1}]^-$ (n = 1, 2) anions. The small amounts of additional $[WF_4(NC_5H_5)_4]^{2+}$ are likely generated upon dismutation of $[WF_5(NC_5H_5)_2]^+$ (Eq. 3) and/or $[WF_5(NC_5H_5)_3]^+$ (Eq. 4).

$$[WF_5(NC_5H_5)_2]^+ \rightleftharpoons \tfrac{1}{2}[WF_4(NC_5H_5)_4]^{2+} + \tfrac{1}{2}WF_6 \quad (3)$$

$$[WF_5(NC_5H_5)_3]^+ \rightleftharpoons \tfrac{1}{2}[WF_4(NC_5H_5)_4]^{2+} + \tfrac{1}{2}WF_6(NC_5H_5)_2 \quad (4)$$

Reaction rates for the four-site exchange process observed in the ^{19}F NMR spectra between –100 °C and 0 °C were determined via dynamic NMR simulations (Figure S6 and Table S6), the Eyring plot of which (Figure S7) yielded precise values for $\Delta H^‡$ (37.8(6) kJ mol^{-1}) and $\Delta S^‡$ (0(3) J mol^{-1} K^{-1}). The process is entropically neutral, suggesting unimolecular exchange that is best described as a rotation of the F_X square face with respect to the triangular face formed by F_A and the Z pyridyl ligands. This mechanism is corroborated by the prediction of such a rotation as a low-frequency vibrational mode (86 cm^{-1}) and would be consistent with the observed averaging of all ^2J coupling to F_A along with loss of through-space coupling from H_O to F_C. As the F_X square face is capped by the Y pyridyl ligand, the proposed exchange mechanism invokes the "monocapped-4:3" coordination sphere used to describe the solid-state geometries of the $[WF_5(L)]^+$ salts.[12]

2.4.2 Decomposition of $[WF_5(NC_5H_5)_3][O_3SCF_3]$ in C_5H_5N

Monitoring the reaction of equimolar WF_6 and $(CH_3)_3SiO_3SCF_3$ in C_5H_5N by ambient-temperature ^{19}F NMR spectroscopy reveals immediate formation of equimolar amounts of $(CH_3)_3SiF$ and $[O_3SCF_3]^-$, along with $[WF_5(NC_5H_5)_3]^+$ and small amounts of $WF_6(NC_5H_5)_2$. After quantitative F^- abstraction, the ratio of the combined integrals of the F-on-W^{VI} resonances, i.e., those for $[WF_5(NC_5H_5)_3]^+$ (165, 129 ppm) and $WF_6(NC_5H_5)_2$ (114 ppm[34]), to the integral of $[O_3SCF_3]^-$ is expected to be 5:3. A ratio of 4.80:3 was observed after *ca.* 15 min, which gradually decreased over time (4.65:3 after *ca.* 30 min; 4.14:3 after *ca.* 90 min), indicating slow reduction of W^{VI} to NMR-silent W^V. After *ca.* 16 h, only $WF_6(NC_5H_5)_2$ was observed.

The $WF_6(NC_5H_5)_2$ adduct is retained due to consumption of $(CH_3)_3SiO_3SCF_3$ via twofold F^- abstraction from WF_6 to form $[WF_4(NC_5H_5)_4]^{2+}$ (Eq. 2) and/or generated by dismutation of $[WF_5(NC_5H_5)_n]^+$ (n = 2, 3; Eqs. 3 and 4). The $[WF_4(NC_5H_5)_4]^{2+}$ and $[WF_5(NC_5H_5)_2]^+$ cations are not observed directly, which is attributed to their rapid reduction in C_5H_5N. This was corroborated

by monitoring a reaction employing 1.5 molar equivalents of $(CH_3)_3SiO_3SCF_3$. Whereas $WF_6(NC_5H_5)_2$ is gradually formed over the course of *ca.* 90 min in the 1:1 reaction as a result of dismutation (Figure S8), in the 1:1.5 reaction, this formation is suppressed, consistent with Eq. 2 suppressing Eqs. 3 and/or 4, while a more significant decrease in cumulative F-on-W^{VI} signal intensity is observed (1.62:3 with respect to $[O_3SCF_3]^-$ after *ca.* 30 min). The dication is apparently not reduced to $WF_5(NC_5H_5)_2$, as the latter did not crystallise appreciably from this solution. It is possible that a monocationic species that remains dissolved in the inextricable oil, such as $[WF_4(NC_5H_5)_4]^+$, is formed. This is reinforced by the observed loss of yield when 1.5 molar equivalents of $(CH_3)_3SiO_3SCF_3$ were used in a preparation of $WF_5(NC_5H_5)_2$. The more pronounced dismutation of $[WF_5(NC_5H_5)_n]^+$ (n = 2, 3) in C_5H_5N than in CH_2Cl_2 is apparently driven by rapid consumption of the dication via reduction.

The ^{1}H NMR spectra revealed formation of $(CH_3)_3SiF$ and the *N*-(4-pyridyl)pyridinium cation ($[4\text{-pypy}]^+$); no additional species developed after 16–24 h at ambient temperature (Figure S9). Formation of $[4\text{-pypy}]^+$ has been observed previously upon reduction of MX_5 (M = Nb, Ta; X = Cl, Br),[38] WBr_5,[39] and WCl_6[39] by C_5H_5N (Eq. 5). Notably, the reduction of these transition-metal halides is proposed to proceed via $[MX_4(NC_5H_5)_2]^+$ cations as reactive intermediates.[38] The absence of $[C_5H_5NH]^+$ in the ^{1}H NMR spectrum reported herein is attributed to rapid exchange of the nitrogen-bound proton between solvent molecules.

$$MX_5 + 3½C_5H_5N \rightarrow MX_4(NC_5H_5)_2 + ½[4\text{-pypy}]X + ½[C_5H_5NH]X \quad (5)$$

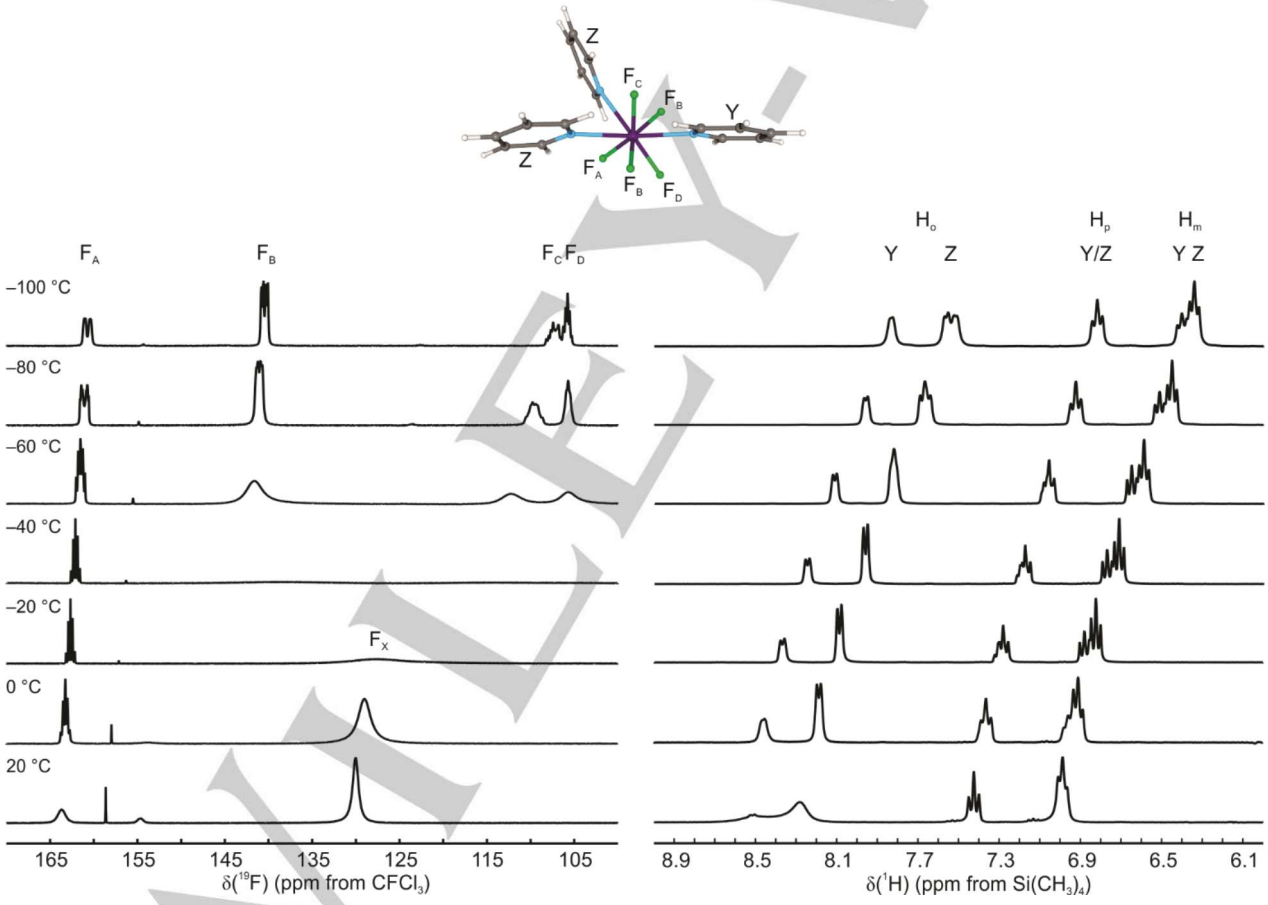

Figure 4. Fluorine-on-tungsten region in the ^{19}F NMR spectra (left) and aromatic-proton region in the ^{1}H NMR spectra (right) of $[WF_5(NC_5H_5)_3][O_3SCF_3]$, recorded in CH_2Cl_2 at various temperatures from –100 to 20 °C.

2.4.3 Attempted Synthesis of $[WF_5(NC_5H_5)_2][Sb_2F_{11}]$ in SO_2

An attempt to prepare $[WF_5(NC_5H_5)_2][Sb_2F_{11}]$ via reaction of $WF_6(NC_5H_5)_2$ with $SbF_5(OSO)$ in SO_2 (Eq. 6) resulted in formation of a yellow solution, in which $[WF_5(NC_5H_5)_2]^+$ was observed by ^{19}F NMR spectroscopy at –50 °C (Figure S10). The $[WF_5(NC_5H_5)_2]^+$ cation, however, is highly susceptible to decomposition, preventing its isolation. In addition to a broad resonance corresponding to the expected cation (205 ppm, *cf.* $[WF_5(L)]^+$: 204–206 ppm),[12] significant amounts of WF_6 (166.96 ppm) and traces of $[WF_4(NC_5H_5)_4]^{2+}$ (157.43 ppm) were observed, along with broad resonances at 243 and 175 ppm that are attributed to unidentified fluoridotungsten(VI) cations. A similar dark brown impurity was observed at 235 ppm in the ^{19}F NMR spectrum of $[WF_5(2,2'\text{-bipy})]^+$, which could be removed by keeping the solution at ambient temperature for *ca.* 16 h.[12] However, while intermittently warming the $[WF_5(NC_5H_5)_2]^+$ solution to ambient temperature resulted in depletion of the broad resonances and complete loss of colour, increased proportions of $[WF_4(NC_5H_5)_4]^{2+}$ and WF_6 were generated at the expense of $[WF_5(NC_5H_5)_2]^+$, revealing its much greater susceptibility to dismutation than $[WF_5(L)]^+$, which are stable as their $[Sb_2F_{11}]^-$ salts.

$$WF_6(NC_5H_5)_2 + 2SbF_5(OSO) \rightarrow [WF_5(NC_5H_5)_2][Sb_2F_{11}] + 2SO_2 \quad (6)$$

The proportion of WF_6 with respect to $[WF_4(NC_5H_5)_4]^{2+}$ increased after several minutes at ambient temperature such that its formation could not be accounted for entirely by dismutation of $[WF_5(NC_5H_5)_2]^+$. This suggests that C_5H_5N abstraction from $WF_6(NC_5H_5)_2$ by $SbF_5(OSO)$ occurs as an additional side reaction (Eq. 7). However, $SbF_5(NC_5H_5)$ could not be unambiguously identified due to possible overlap between resonances that would correspond to it (assuming similarities to $SbF_5(NCR)$ adducts[40]), $SbF_5(OSO)$,[41] and $[Sb_2F_{11}]^-$[41] (Figure S11).

$$WF_6(NC_5H_5)_2 + 2SbF_5(OSO) \rightarrow WF_6 + 2SbF_5(NC_5H_5) + 2SO_2 \quad (7)$$

It should be noted that there was no evidence for formation of $[4\text{-pypy}]^+$ or $[C_5H_5NH]^+$ in the attempted synthesis of $[WF_5(NC_5H_5)_2][Sb_2F_{11}]$, nor discolouration of the sample even after storage at ambient temperature for 24 h. This illustrates the necessity of free C_5H_5N for reduction of the cation to occur.

2.5. Molecular Orbitals and Natural-Bond-Orbital (NBO) Analysis of $[WF_5(NC_5H_5)_n]^+$ (n = 2, 3) and $WF_5(NC_5H_5)_2$

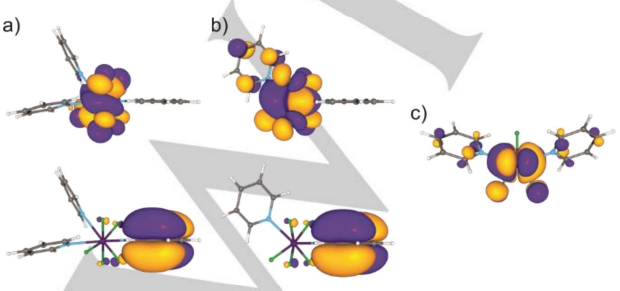

Figure 5. LUMO (top) and HOMO (bottom) of a) $[WF_5(NC_5H_5)_3]^+$ and b) $[WF_5(NC_5H_5)_2]^+$, with c) the SOMO of $WF_5(NC_5H_5)_2$. Isosurface values are drawn at 0.02 e Å^{-3}.

The HOMO-LUMO transitions of $[WF_5(NC_5H_5)_n]^+$ (n = 2, 3) are predicted to be ligand-to-metal charge transfer in nature (Figures 5a and 5b). However, in the LUMO of $[WF_5(NC_5H_5)_2]^+$, there is also substantial $p_\pi(C_o)$ and $p_\pi(C_p)$ character on the non-capping pyridyl ligand. The HOMO-LUMO gaps of the cations (n = 2: 3.76 eV; n = 3: 4.09 eV) are comparable to those calculated for $[WF_5(L)]^+$ (L = 2,2′-bipy, 1,10-phen; 3.66–3.92 eV) at the same level of theory,[12] despite the difference in colour between the cations bearing bidentate (yellow-orange) vs. monodentate ligands (colourless). The LUMO energy of $[WF_5(NC_5H_5)_2]^+$ (–7.63 eV) is significantly lower than that of $[WF_5(NC_5H_5)_3]^+$ (–6.60 eV), suggesting a much greater susceptibly of the former to reduction. For comparison, the difference in LUMO energies is similar to the difference in EAs between MoF_6 (4.23 eV[42]) and WF_6 (3.16 eV[6]); the former is capable of oxidising NO to $[NO]^+$, whereas the latter is not.[43] The SOMO of $WF_5(NC_5H_5)_2$, like the LUMO of its parent cation, possesses $\pi^*(d(W)–p(F))$ and $p_\pi(C)$ character (Figure 5c). The absence of $\sigma^*(d(W)–p(N))$ interactions explains the observed insignificant change in the W–N bond lengths in $WF_5(NC_5H_5)_2$ while the W–F bonds are elongated upon comparison to related W^{VI} complexes.

Table 2. Selected NPA Charges and WBIs of $[WF_5(NC_5H_5)_n]^+$ (n = 2, 3) and $WF_5(NC_5H_5)_2$[a]

	$[WF_5(NC_5H_5)_3]^+$	$[WF_5(NC_5H_5)_2]^+$	$WF_5(NC_5H_5)_2$
W	+2.48	+2.57	+2.31
F	–0.47 to –0.51	–0.45 to –0.46	–0.54 to –0.57
N	–0.45 to –0.46	–0.48 to –0.50	–0.46
$\Sigma(C_5H_5N)$	+0.30 to +0.32	+0.35 to +0.36	+0.23
W–F	0.69 to 0.75	0.75 to 0.80	0.65 to 0.68
W–N	0.40 to 0.42	0.45 to 0.46	0.38
W–N/W–F	0.53 to 0.61	0.56 to 0.61	0.56 to 0.58

[a] Calculated at the B3LYP/aVTZ level of theory.

Natural-bond-orbital (NBO) analyses were performed, providing natural-population-analysis (NPA) charges, Wiberg valences, and Wiberg bond indices (WBIs) for $[WF_5(NC_5H_5)_n]^+$ (n = 2, 3) and $WF_5(NC_5H_5)_2$ (Tables 2 and S7). There is a large degree of compensatory electron donation from the pyridyl ligands to stabilise the electron-poor W^{VI} centres of $[WF_5(NC_5H_5)_n]^+$ (n = 2, 3), as evidenced by the cumulative NPA charges on the ligands, which in the case of $[WF_5(NC_5H_5)_3]^+$ (+0.92), accounts for nearly all of the overall charge of the complex. Correspondingly, the NPA charge on the W^{VI} centre decreases only slightly upon reduction to W^V (+2.57 → +2.31). The WBIs of the W–F and W–N bonds in $[WF_5(NC_5H_5)_2]^+$ (n = 2, 3) are similar to $[WF_5(L)]^+$ (W–F: 0.79–0.83, W–N: 0.42), with the W–F bonds being slightly weaker and the W–N bonds slightly stronger. Meanwhile, those of $[WF_5(NC_5H_5)_3]^+$ are more similar to $WF_6(NC_5H_5)$ and derivatives thereof (W–F: 0.71–0.77, W–N: 0.31–0.40). In the case of both $[WF_5(NC_5H_5)_n]^+$ cations, the W–N bonds strengths are somewhat more than half those of the W–F bonds (W–N/W–F: 0.53–0.61).

The WBIs of $WF_5(NC_5H_5)_2$ suggest proportional weakening of the W–F and W–N bonds (W–N/W–F: 0.56–0.58) with respect to $[WF_5(NC_5H_5)_2]^+$. Significant $\sigma(lp(N)\rightarrow lv(W))$ (lp = lone pair, lv = lone valence) bonding (324 kJ mol^{-1} per ligand) is predicted for

$WF_5(NC_5H_5)_2$ as per second-order perturbation analysis of the NBO donor-acceptor interactions, whereas there exists negligible synergic bonding in the form of π (lp(W)→π*(NC)) interactions (<5 kJ mol^{-1} per ligand), consistent with the highly positive NPA charge on the electron-poor W^V centre (+2.31).

2.6 Thermodynamics of the Reduction of $[WF_5(NC_5H_5)_2]^+$

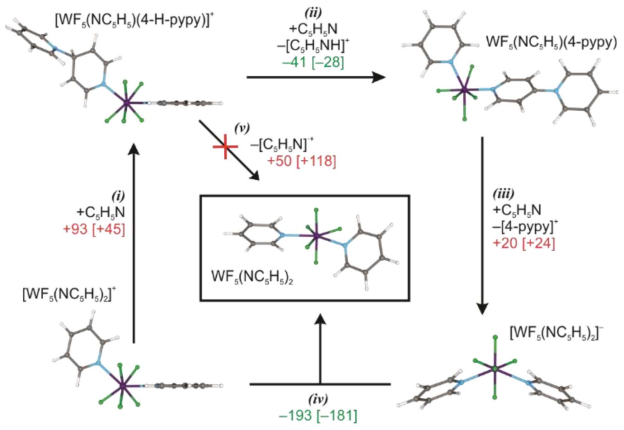

Scheme 1. Proposed routes for the reduction of $[WF_5(NC_5H_5)_2]^+$ in C_5H_5N, with optimised geometries and calculated Gibbs energies [enthalpies] (kJ mol^{-1}) in C_5H_5N at 25 °C (B3LYP/aVTZ).

Considering that nucleophilic attack at a pyridyl ligand is the proposed first step for the reduction of transition-metal halides by C_5H_5N[38] and the LUMO of $[WF_5(NC_5H_5)_2]^+$ could facilitate such an attack, the thermodynamic feasibility of a similar route for the reduction of $[WF_5(NC_5H_5)_2]^+$ was investigated at the B3LYP/aVTZ level of theory. The reactions characterised for the reduction of $[WF_5(NC_5H_5)_2]^+$ by C_5H_5N are illustrated in Scheme 1, with structures and Gibbs energies calculated in implicit C_5H_5N solvent (SMD solvent model) at 25 °C. Gas-phase thermochemical data are given in Table S8 and Gibbs energies and enthalpies of solvation are given in Table S9.

First, it was established that dissociation of C_5H_5N from $[WF_5(NC_5H_5)_3]^+$ (Eq. 8) is thermodynamically favourable (Δ_rG = –33 kJ mol^{-1}, Δ_rH = +13 kJ mol^{-1}), which is consistent with the ^{19}F NMR spectroscopic studies. Furthermore, an attempt to optimise the intermediate complex formed upon nucleophilic attack at a *para* carbon atom in $[WF_5(NC_5H_5)_3]^+$ was unsuccessful, as the C_p–N bond of the intermediate preferentially dissociated to regenerate the parent cation and free C_5H_5N. These observations corroborate the notion that $[WF_5(NC_5H_5)_3]^+$ is not directly involved in the redox process.

$$[WF_5(NC_5H_5)_3]^+ \rightleftharpoons [WF_5(NC_5H_5)_2]^+ + C_5H_5N \quad (8)$$

Nucleophilic attack at the activated *para* carbon atom of $[WF_5(NC_5H_5)_2]^+$, meanwhile, is predicted to result in an intermediate 4-hydro-4-(1′-pyridyl)pyridyl (4-H-pypy) complex (Scheme 1, (i)). The optimised gas-phase structure of this intermediate reveals that the coordination geometry of the W^{VI} centre does not change. However, complete dearomatisation of the attacked pyridyl ligand results in a semiquinoidal complex with a W=N bond, causing significant contraction of the W–N (2.108 Å) and C_o–C_m bonds (1.344, 1.345 Å) and complementary elongation of the C_o–N (1.352, 1.359 Å) and C_m–C_p (1.397, 1.403 Å) bonds with respect to $[WF_5(NC_5H_5)_2]^+$ (Table S3). The formation of a W=N bond indicates that 4-H-pypy is redox non-innocent, whereas the ligand-centred HOMOs of $[WF_5(NC_5H_5)_n]^+$ (n = 2, 3; Figures 5a and 5b) suggest innocence from the pyridyl ligands.

The reduction of $[WF_5(NC_5H_5)_2]^+$ could proceed through $[WF_5(NC_5H_5)(4\text{-H-pypy})]^+$ as a reactive intermediate, despite its thermodynamic unfavourability, assuming rapid deprotonation of 4-H-pypy by free C_5H_5N (Scheme 1, (ii)). This results in concomitant rearomatisation of 4-H-pypy to $[4\text{-pypy}]^+$ and formal two-electron reduction of W^{VI} to afford a zwitterionic W^{IV} complex, $WF_5(NC_5H_5)(4\text{-pypy})$. This complex is predicted to adopt a pentagonal-bipyramidal geometry in which the $[4\text{-pypy}]^+$ ligand occupies an axial position, in contrast to the co-equatorial positions of the pyridyl ligands in $WF_5(NC_5H_5)_2$.

Following reduction from W^{VI} to W^{IV}, substitution of the $[4\text{-pypy}]^+$ ligand with C_5H_5N is expected to occur (Scheme 1, (iii)), after which a highly exergonic and exothermic comproportionation of the resultant $[WF_5(NC_5H_5)_2]^-$ with $[WF_5(NC_5H_5)_2]^+$ would yield the final product (Scheme 1, (iv)). The overall one-electron reduction of $[WF_5(NC_5H_5)_2]^+$ to $WF_5(NC_5H_5)_2$ via the proposed route (Eq. 9) is predicted to be thermodynamically favourable (Δ_rG = –60 kJ mol^{-1}, Δ_rH = –70 kJ mol^{-1}).

$$[W^{VI}F_5(NC_5H_5)_2]^+ + 1\tfrac{1}{2}C_5H_5N \rightarrow W^{V}F_5(NC_5H_5)_2 + \tfrac{1}{2}[C_5H_5NH]^+ + \tfrac{1}{2}[4\text{-pypy}]^+ \quad (9)$$

In lieu of the multi-step mechanism described, direct reduction from W^{VI} to W^V could be envisioned via homolysis of the C_p–N bond in $[WF_5(NC_5H_5)(4\text{-H-pypy})]^+$ (Scheme 1, (v)). However, this reaction is unfavourable with respect to the already unstable intermediate and especially with respect to $[WF_5(NC_5H_5)_2]^+$ in C_5H_5N (Scheme 1, (i) + (v); Δ_rG = +143 kJ mol^{-1}, Δ_rH = +163 kJ mol^{-1}). In addition, it is inconsistent with the observed ^1H NMR spectrum; a radical-substitution reaction of C_5H_5N with $[C_5H_5N]^{\bullet+}$ would necessarily be termolecular in nature and expected to result in a mixture of isomers (Eq. 10), as was observed during analogous reactions of C_5H_5N with 2-$C_6H_4R^{\bullet}$ (R = H, CH_3, NO_2).[44]

$$2[C_5H_5N]^{\bullet+} + C_5H_5N \rightarrow [x\text{-pypy}]^+ + [C_5H_5NH]^+ \ (x = 2, 3, 4) \quad (10)$$

3 Conclusions

Though $[WF_5(NC_5H_5)_2]^+$ was found to be much less stable towards dismutation than $[WF_5(L)]^+$ (L = 2,2′-bipy, 1,10-phen), the $[O_3SCF_3]^-$ salt of trigonal-dodecahedral $[WF_5(NC_5H_5)_3]^+$ could be stabilised at ambient temperature in the solid state and below 0 °C in solution. Above 0 °C, the cation is prone to dissociation of a pyridyl ligand in solution that, in the presence of excess C_5H_5N, results in the rapid reduction of transiently generated $[WF_5(NC_5H_5)_2]^+$ to $WF_5(NC_5H_5)_2$, as determined by ^{19}F and ^1H NMR spectroscopy. The $WF_5(NC_5H_5)_2$ adduct is the first unambiguously characterised WF_5 adduct and heptacoordinate MF_5 adduct (for any transition metal M), the pentagonal-bipyramidal geometry of which was confirmed by X-ray crystallography. The thermal stability of this adduct suggests an accessible point of entry into the chemistry of tungsten(V) fluorides, considering the difficulty in preparing and isolating the parent WF_5. Computational studies affirmed that whereas

$[WF_5(NC_5H_5)_3]^+$ is reductively resistant towards C_5H_5N, $[WF_5(NC_5H_5)_2]^+$ undergoes two-electron reduction via activation of the para carbon atom of a pyridyl ligand, followed by comproportionation to W^V.

Acknowledgements

We thank the Natural Sciences and Engineering Research Council of Canada for awarding Discovery grants to P. H., S.D.W. and M.G. as well as CGS-M and PGS-D scholarships to D.T. In addition, we thank the University of Lethbridge for awarding the SGS Dean's Scholarship and Tuition Award to D.T. and supporting this work. The computational studies were performed using equipment funded through the Canada Foundation of Innovation, as well as resources made available through Westgrid and Compute/Calcul Canada.

Keywords: Fluorine • Lewis acids • Tungsten • Redox chemistry • X-ray crystallography

[1] N. Bartlett, D. H. Lohmann, *J. Chem Soc.* **1962**, 5253.
[2] N. Bartlett, *Proc. Chem Soc.* **1962**, 218.
[3] L. Graham, O. Graudejus, N. K. Jha, N. Bartlett, *Coord. Chem Rev.* **2000**, *197*, 321–334.
[4] F. P. Gortsema, R. H. Toeniskoetter, *Inorg. Chem* **1966**, *5*, 1217–1222.
[5] N. Bartlett, *Angew. Chem Int. Ed. Engl.* **1968**, *7*, 433–439.
[6] R. Craciun, D. Picone, R. T. Long, S. Li, D. A. Dixon, K. A. Peterson, K. O. Christe, *Inorg. Chem* **2010**, *49*, 1056–1070.
[7] H. Shorafa, D. Mollenhauer, B. Paulus, K. Seppelt, *Angew. Chem Int. Ed.* **2009**, *48*, 5845–5847.
[8] F. Tamadon, S. Seidel, K. Seppelt, *Acta Chim Slov.* **2013**, *60*, 491–494.
[9] R. Bougon, P. Cearpin, *J. Fluorine Chem* **1979**, *14*, 235–241.
[10] G. S. H. Chen, J. Passmore, P. Taylor, T. K. Whidden, *Inorg. Nucl. Chem Lett.* **1976**, *12*, 943–948.
[11] G. S. H. Chen, J. Passmore, P. Taylor, T. K. Whidden, P. S. White, *J. Chem Soc. Dalt. Trans.* **1985**, 9–16.
[12] D. Turnbull, S. D. Wetmore, M. Gerken, *Angew. Chem Int. Ed.* **2019**, *58*, 13035–13038.
[13] J. Schröder, F. J. Grewe, *Angew. Chem Int. Ed. Engl.* **1968**, *7*, 132–133.
[14] J. Schröder, F. J. Grewe, *Chem Ber.* **1970**, *103*, 1536–1546.
[15] T. A. O'Donnell, T. E. Peel, *J. Inorg. Nucl. Chem* **1976**, *28*, 61–62.
[16] E. Lassner, W.-D. Schubert, *Int. J. Refract. Met. Hard Mater.* **1995**, *13*, 111–117.
[17] L. Arnaudet, R. Bougon, B. Ban, P. Charpin, J. Isabey, M. Lance, M. Nierlich, J. Vigner, *Inorg. Chem* **1989**, *28*, 257–262.
[18] D. Turnbull, S. D. Wetmore, M. Gerken, *Inorg. Chem* **2019**, *58*, 6363–6375.
[19] J. W. Emsley, W. Levason, G. Reid, W. Zhang, G. De Luca, *J. Fluorine Chem* **2017**, *197*, 74–79.
[20] S. E. Eklund, J. Q. Chambers, G. Mamantov, J. Diminnie, C. E. Barnes, *Inorg. Chem* **2001**, *40*, 715–722.
[21] L. Arnaudet, R. Bougon, B. Ban, M. Lance, M. Nierlich, J. Vigner, *Inorg. Chem* **1993**, *32*, 1142–1146.
[22] D. Turnbull, N. Kostiuk, S. D. Wetmore, M. Gerken, *J. Fluorine Chem* **2018**, *215*, 1–9.
[23] S. El-Kurdi, A.-A. Al-Terkawi, B. Schmidt, A. Dimitrov, K. Seppelt, *Chem Eur. J.* **2010**, *16*, 595–599.
[24] P. Scilabra, G. Terraneo, G. Resnati, *J. Fluorine Chem* **2017**, *203*, 62–74.
[25] K. C. Moss, *J. Chem Soc. A* **1970**, 1224–1226.
[26] J. A. S. Howell, K. C. Moss, *J. Chem Soc. A* **1971**, 2483–2487.
[27] R. Haiges, P. Deokar, K. O. Christe, *Z. Anorg. Allg. Chem* **2014**, *640*, 1568–1575.
[28] F. Marchetti, G. Pampaloni, *Chem Commun.* **2012**, *48*, 635–653.
[29] W. Levason, F. M. Monzittu, G. Reid, *Coord. Chem Rev.* **2019**, *391*, 90–130.
[30] L. Arnaudet, R. Bougon, B. Buu, M. Lance, M. Nierlich, J. Vigner, *Inorg. Chem* **1994**, *33*, 4510–4516.
[31] B. Scheibe, S. S. Rudel, M. R. Buchner, A. J. Karttunen, F. Kraus, *Chem Eur. J.* **2017**, *23*, 291–295.
[31] J. K. Burdett, R. Hoffmann, R. C. Fay, *Inorg. Chem* **1978**, *17*, 2553–2568.
[32] M. Sampoli, N. C. Marziano, C. Tortato, *J. Phys. Chem* **1989**, *93*, 7252–7257.
[33] L. Arnaudet, R. Bougon, B. Buu, M. Lance, M. Nierlich, P. Thuéry, J. Vigner, *J. Fluorine Chem* **1995**, *71*, 123–129.
[34] L. Arnaudet, R. Bougon, B. Ban, M. Lance, A. Navaza, M. Nierlich, J. Vigner, *J. Fluorine Chem* **1994**, *67*, 17–25.
[35] L. Arnaudet, R. Bougon, B. Ban, M. Lance, A. Navaza, M. Nierlich, J. Vigner, *J. Fluorine Chem* **1992**, *59*, 141–152.
[36] R. E. McCarley, B. G. Hughes, J. C. Boatman, B. A. Torp, in *Reactions of Coordinated Ligands and Homogeneous Catalysis*, American Chemical Society, **1963**, pp. 243–255.
[37] SpinWorks, version 4.2.7. K. Marat, University of Manitoba, Winnipeg, MB, CA, **2017**.
[38] R. E. McCarley, T. M. Brown, *Inorg. Chem* **1964**, *3*, 1232–1236.
[39] T. Saal, K. O. Christe, R. Haiges, *Dalton Trans.* **2019**, *48*, 99–106.
[40] J. Bacon, P. A. W. Dean, R. J. Gillespie, *Can. J. Chem* **1969**, *47*, 1655–1659.
[41] R. Craciun, R. T. Long, D. A. Dixon, K. O. Christe, *J. Phys. Chem A* **2010**, *114*, 7571–7582.
[42] J. R. Geichman, E. A. Smith, S. S. Trond, P. R. Ogle, *Inorg. Chem* **1962**, *1*, 661–665.
[43] R. A. Abramovitch, J. G. Saha, *J. Chem Soc.* **1964**, *0*, 2175–2187.
[44] J. M. Winfield, *J. Fluorine Chem* **1984**, *25*, 91–98.

Entry for the Table of Contents

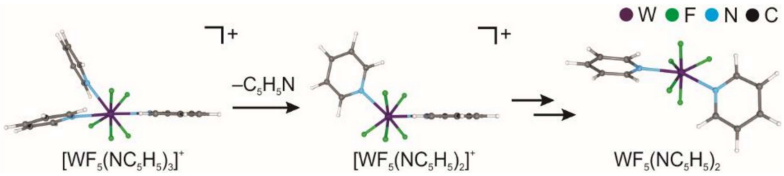

Trigonal-dodecahedral $[WF_5(NC_5H_5)_3]^+$ was isolated as its $[O_3SCF_3]^-$ salt and its geometry was predicted by DFT calculations, which was confirmed by NMR spectroscopy at –100 °C. It dissociates to $[WF_5(NC_5H_5)_2]^+$, which is reduced in C_5H_5N to ambient-temperature stable $WF_5(NC_5H_5)_2$. The crystal structure of $WF_5(NC_5H_5)_2$ reveals a pentagonal-bipyramidal geometry and its synthesis provides an accessible point of entry into the chemistry of unstable WF_5.